Table 2 Results for the ^{7}Li/^{6}Li ratio, the total Li/H abundance and the K/Li abundance ratio

Parameter	o Per	ζ Per
^{7}Li/^{6}Li ratio	3.6 ± 0.6 1.7 ± 0.3	10.6 ± 2.9
Li/H abundance	$(9.8 \pm 3.5) \times 10^{-10}$	$(12.2 \pm 2.2) \times 10^{-10}$
K/Li abundance ratio	65 ± 4 48 ± 4	42 ± 2

For our estimates of the total Li/H abundance, the electron density (n_e) is obtained from N(C II), the total proton column density [N(H) = N(H I) + 2N(H_2)], and the gas density (n). Since no precise N(C II) measurements exist for the direction toward o Per, the weighted mean interstellar ratio[24] of N(C II)/N(H) = $(1.42 \pm 0.13) \times 10^{-4}$ was utilized, yielding N(C II) = $(2.2 \pm 0.8) \times 10^{17}$ cm^{-2}. The value of N(C II) is $(1.84 \pm 0.32) \times 10^{17}$ cm^{-2} toward ζ Per (ref. 25). The columns N(H) (refs 26, 27) are $(15.2 \pm 5.3) \times 10^{20}$ cm^{-2} toward o Per and $(15.8 \pm 4.7) \times 10^{20}$ cm^{-2} toward ζ Per. Chemical models for carbon-bearing molecules[28] indicate values for n of 800 and 700 cm^{-3} toward o and ζ Per, respectively. The total Li/H abundance is derived from {[N(^{7}Li I) + N(^{6}Li I)]/N(H)} × [G/(αn_e)], where a value of 41 was used for $(G/\alpha)_{Li}$, the photoionization rate to recombination rate coefficient[18]. The ionization corrections for the two clouds toward o Per are assumed to be the same. The K/Li ratios are based on column densities in Table 1 and a value of 9.4 for $(G/\alpha)_K$ (ref. 18). For the ^{7}Li/^{6}Li and K/Li ratios toward o Per, component 1 is the first entry and component 2 is the second.

The presence of deuterium as HD molecules toward o Per (ref. 21) implies that the gas within the superbubble cannot have been totally depleted in Li initially. The D-containing gas may be largely in the cloud for which we find ^{7}Li/^{6}Li ≈ 4. Synthesis of D within a superbubble is negligible. The existence of D may warrant consideration of alternative hypotheses, including (1) isotopic fractionation of Li in diffuse clouds and (2) the idea that pristine interstellar gas has ^{7}Li/^{6}Li ≈ 2, the value for cosmic ray spallation, and so varying degrees of contamination with ejecta from Li-rich red giants drive the ratio to the higher values seen in ζ Per's clouds and elsewhere. □

Received 18 February; accepted 19 April 2000.

1. Reeves, H., Fowler, W. A. & Hoyle, F. Galactic cosmic ray origin of Li, Be and B in stars. *Nature* **226,** 727–729 (1970).
2. Meneguzzi, M., Audouze, J. & Reeves, H. The production of the elements Li, Be, B by galactic cosmic rays in space and its relation with stellar observations. *Astron. Astrophys.* **15,** 337–359 (1971).
3. Meneguzzi, M. & Reeves, H. Light element production by cosmic rays. *Astron. Astrophys.* **40,** 99–110 (1975).
4. Ramaty, R., Kozlovsky, B. & Lingenfelter, R. E. Light isotopes, extinct radioisotopes, and gamma-ray lines from low-energy cosmic-ray interactions. *Astrophys. J.* **456,** 525–540 (1996).
5. Lemoine, M., Vangioni-Flam, E. & Cassé, M. Galactic cosmic rays and the evolution of light elements. *Astrophys. J.* **499,** 735–745 (1998).
6. Anders, E. & Grevesse, N. Abundances of the elements: meteoritic and solar. *Geochim. Cosmochim. Acta* **53,** 197–214 (1989).
7. Chaussidon, M. & Robert, F. ^{7}Li/^{6}Li and ^{11}B/^{10}B variations in chondrules from the Semarkona unequilibrated chondrite. *Earth Planet. Sci. Lett.* **164,** 577–589 (1998).
8. Tull, R. G., MacQueen, P. J., Sneden, C. & Lambert, D. L. The high resolution cross-dispersed echelle white-pupil spectrometer of the McDonald Observatory 2.7 m telescope. *Publ. Astron. Soc. Pacif.* **107,** 251–264 (1995).
9. Lemoine, M., Ferlet, R., Vidal-Madjar, A., Emerich, C. & Bertin, P. Interstellar lithium and the ^{7}Li/^{6}Li ratio toward ρ Oph. *Astron. Astrophys.* **269,** 469–476 (1993).
10. Lemoine, M., Ferlet, R. & Vidal-Madjar, A. The interstellar ^{7}Li/^{6}Li ratio. The line of sight to ζ Ophiuchi. *Astron. Astrophys.* **298,** 879–893 (1995).
11. Morton, D. C. Atomic data for resonance absorption lines. I. Wavelengths longward of the Lyman limit. *Astrophys. J. Suppl.* **77,** 119–202 (1991).
12. Federman, S. R., Lambert, D. L., Cardelli, J. A. & Sheffer, Y. The boron isotope ratio in the interstellar medium. *Nature* **381,** 764–766 (1995).
13. Lambert, D. L. *et al.* The ^{11}B/^{10}B ratio of local interstellar diffuse clouds. *Astrophys. J.* **494,** 614–622 (1998).
14. Meyer, D. M., Hawkins, I. & Wright, E. L. The interstellar ^{7}Li/^{6}Li isotope ratio toward ζ Ophiuchi and ζ Persei. *Astrophys. J.* **409,** L61–L64 (1993).
15. van Dishoeck, E. F. & Black, J. H. Comprehensive models of diffuse interstellar clouds: Physical conditions and molecular abundances. *Astrophys. J. Suppl.* **62,** 109–145 (1986).
16. Federman, S. R., Weber, J. & Lambert, D. L. Cosmic ray-induced chemistry toward Perseus OB2. *Astrophys. J.* **463,** 181–190 (1996).
17. Crane, P., Lambert, D. L. & Sheffer, Y. A very high resolution survey of interstellar CH and CH^+. *Astrophys. J. Suppl.* **99,** 107–120 (1995).
18. White, R. E. Interstellar lithium: differential depletion in diffuse clouds. *Astrophys. J.* **307,** 777–786 (1986).
19. Andersen, J., Gustafsson, B. & Lambert, D. L. The lithium isotope ratio in F and G stars. *Astron. Astrophys.* **136,** 65–73 (1984).
20. Parizot, E. & Drury, L. Superbubbles as the source of ^{6}Li, Be, and B in the early Galaxy. *Astron. Astrophys.* **349,** 673–684 (1999).
21. Snow, T. P. Jr Interstellar molecular abundances toward omicron Persei. *Astrophys. J.* **201,** L21–L24 (1975).
22. Sansonetti, C. J., Richou, B., Engleman, R. Jr & Radziemski, L. J. Measurements of the resonance lines of ^{6}Li and ^{7}Li by Doppler-free frequency-modulation spectroscopy. *Phys. Rev. A* **52,** 2682–2688 (1995).
23. Hobbs, L. M., Thorburn, J. A. & Rebull, L. M. Lithium isotope ratios in halo stars. III. *Astrophys. J.* **523,** 797–804 (1999).
24. Sofia, U. J., Cardelli, J. A., Guerin, K. P. & Meyer, D. M. Carbon in the diffuse interstellar medium. *Astrophys. J.* **482,** L105–L108 (1997).
25. Cardelli, J. A., Meyer, D. M., Jura, M. & Savage, B. D. The abundance of interstellar carbon. *Astrophys. J.* **467,** 334–340 (1996).
26. Savage, B. D., Bohlin, R. C., Drake, J. F. & Budich, W. A survey of interstellar molecular hydrogen. *Astrophys. J.* **216,** 291–307 (1977).
27. Diplas, A. & Savage, B. D. An IUE survey of interstellar H I Lyα absorption. I. Column densities. *Astrophys. J. Suppl.* **93,** 211–228 (1994).
28. Federman, S. R. *et al.* Chemical transitions for interstellar C_2 and CN in cloud envelopes. *Astrophys. J.* **424,** 772–792 (1994).

Acknowledgements

We thank E. Parizot and H. Reeves for fruitful discussions. This work was supported by the National Aeronautics and Space Administration. We made use of the Simbad database, operated at Centre de Donées Astronomiques de Strasbourg, Strasbourg, France.

Correspondence and requests for materials should be addressed to S.R.F. (e-mail: sfederm@uoft02.utoledo.edu).

Correlated electron emission in multiphoton double ionization

Th. Weber*, H. Giessen†, M. Weckenbrock*, G. Urbasch†, A. Staudte*, L. Spielberger*, O. Jagutzki*, V. Mergel*, M. Vollmer† & R. Dörner*

* *Institut für Kernphysik, Universität Frankfurt, August Euler Strasse 6, D-60486 Frankfurt, Germany*
† *Fachbereich Physik, Philipps-Universität, Renthof 5, D-35032 Marburg, Germany*

Electronic correlations govern the dynamics of many phenomena in nature, such as chemical reactions and solid state effects, including superconductivity. Such correlation effects can be most clearly investigated in processes involving single atoms. In particular, the emission of two electrons from an atom—induced by the impact of a single photon[1], a charged particle[2] or by a short laser pulse[3]—has become the standard process for studies of dynamical electron correlations. Atoms and molecules exposed to laser fields that are comparable in intensity to the nuclear fields have extremely high probabilities for double ionization[4,5]; this has been attributed to electron–electron interaction[3]. Here we report a strong correlation between the magnitude and the direction of the momentum of two electrons that are emitted from an argon atom, driven by a femtosecond laser pulse (at 38 TW cm^{-2}). Increasing the laser intensity causes the momentum correlation between the electrons to be lost, implying that a transition in the laser–atom coupling mechanism takes place.

The interaction of superstrong laser fields with matter has a wide range of applications, from surgery to ignition of nuclear fusion; however, there are still many open questions concerning the underlying fundamental physical processes of this interaction. An extremely clean way to address them is to place just one single atom in the laser focus and examine its reaction. In many cases, the response of the atom to the strong laser field can be well understood by considering only one of its electrons to be active; however, one important experimental observation withstands explanation in such simple terms: the production of doubly and multiply charged ions is more effective by many orders of magnitude than predicted by an independent-electron model[4,5]. After this discovery, it was agreed that models were needed that include electron–electron correlation to explain this enhanced multiple ionization rate. Intense efforts to model the two-electron process of double ionization in a laser field have reproduced the main feature of a knee

structure in the double ionization yield as a function of laser peak intensity[6–11] and, moreover, yielded quantitative agreement with the experiment in some cases[12,13].

The physical mechanism behind this nonsequential process is, however, still debatable. The most widely accepted model is a re-scattering mechanism[6,14] in which the first electron is accelerated by the laser field and later driven back by the field towards its parent ion. The second electron is then liberated in an electron–ion impact ionization (for example, see refs 6, 8–10 and 15 for arguments supporting this model and refs 7 and 16 for those opposing it). Alternatively, Fittinghoff *et al.*[4] suggested that the second electron is shaken off by the same mechanism as in double ionization by a single high-energy photon (for example, from synchrotron radiation). Recently, Becker and Faisal[12,17] suggested a model of an energy-sharing mechanism using Coulomb correlation represented by a single Feynman diagram. Strong experimental evidence supporting the re-scattering/energy-sharing mechanism is provided by the suppression of double ionization in elliptically polarized laser fields[15].

Here we report the direct experimental observation of strong electron–electron correlation in the final state. We show that the momentum of one electron strongly depends on the momentum of the other electron. Such coincident electron momentum distributions serve as a detailed testing ground for the opposing theoretical approaches. But they also yield direct and intuitive insight into the dynamics of the laser–atom interaction and shed light on the mechanism leading to double ionization. They answer the question of whether the two electrons are pulled by the laser field to the same side and whether the electron–electron repulsion pushes them to opposite sites. The latter is observed with synchrotron radiation at high photon energies, where the energy of just one photon is sufficient to liberate both electrons[1].

A first step towards differential information on the correlated multiple ionization in strong fields has been gained by observing the momentum distribution of the doubly charged ions for helium[18], argon[19] and neon targets[20]. All three studies found large ion momenta which do not peak at zero, highlighting the correlated nature of the process. In contrast, single ionization, and thus any uncorrelated process[19], gives maximum ion yield at zero momentum.

We have used the well-established technique of cold target recoil ion momentum spectroscopy (COLTRIMS; see refs 21 and 22 for reviews) for the experiment. The linearly polarized light from a Ti-sapphire laser (800 nm, 220-fs pulse width) was focused by a 5-cm focal length lens onto a pre-cooled supersonic argon gas jet.

The ions and electrons were guided by an electric field to opposite sides towards two position-sensitive channel plate detectors with delay-line readout. Their momenta were determined from the flight times and the positions of impact. For more details of the experimental setup and data analysis see ref. 23. The polarization axis of the light was parallel to the electric field and perpendicular to the direction of the gas jet. The peak laser intensity was determined by measurements of ion yield to an estimated accuracy of 15%.

The local argon pressure in the gas jet was adjusted such that the average ion count rate was about 0.04–0.08 per shot. The simultaneously measured coincidence between Ar^+ ions and electrons allowed an online monitoring of the fraction of false coincidences, in which the detected ion and electron are produced in the same laser shot but do not come from the same atom. Such events (about 30% of the total counts) are localized outside the diagonal line in Fig. 1. The contribution of false coincidences has been subtracted from the Ar^{2+}-electron coincidence data; however, this background correction changes only the details, and not the principal findings of our results.

The localization of the correlated events on the diagonal line shows that the momenta of the Ar^+ ion and electron are equal and have opposite signs for each single event. This proves that the laser pulse is short enough to prevent the electron from leaving the focus during the pulse. The momentum transfer from the optical field to the electron and Ar^+ ion is therefore equal and opposite, at every individual time interval and thus for the whole pulse duration. The laser does not pass on significant net momentum to the electron–ion system. The photon momentum is negligible on the scale of interest here, as 1.5 eV photons have a momentum of only 0.0004 a.u. (atomic units: 1 a.u. of momentum is equivalent to 1.995×10^{-24} kg m s^{-1}). This is essential in this experiment, because it ensures that for double ionization the ion momentum $\mathbf{k}_{ion}$ is given by the sum of the two electron momentum vectors $\mathbf{k}_{e1,2}$, $\mathbf{k}_{ion} = -(\mathbf{k}_{e1} + \mathbf{k}_{e2})$. We therefore measured $\mathbf{k}_{ion}$ and the momentum of one of the electrons and could then deduct the momentum of the second electron from momentum conservation. The horizontal line structure that is visible in Fig. 1 results from above-threshold ionization peaks (for example, ref. 24). These peaks are resolved for slow electrons, whereas they are neither resolved for

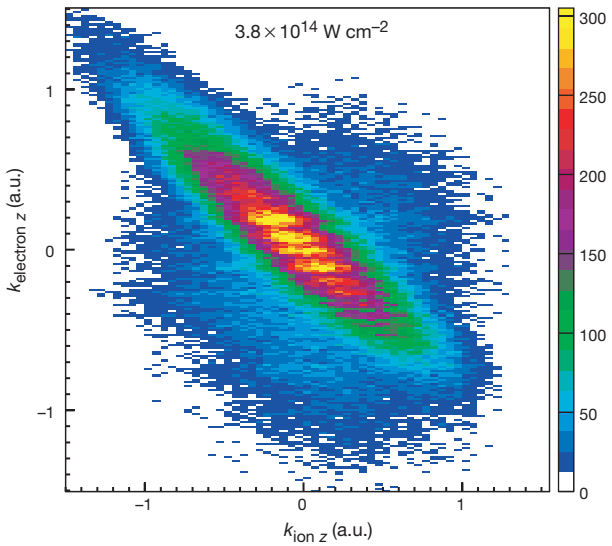

Figure 1 Momentum correlation between the Ar^+ ion and electrons created in the focus of a 220-fs, 800-nm laser pulse at peak intensities of 3.8×10^{14} W cm^{-2}. The horizontal axis shows the momentum component of the Ar^+ ion along the polarization of the laser field; the vertical axis shows the shows the corresponding momentum component of the detected electron.

the ion momenta nor for faster electrons, because we used a time-of-flight technique. The overall resolution (the width of the diagonal of momentum conservation) is about 0.4 a.u. (full-width at half-maximum).

The main result of our work is shown in Fig. 2. The vertical axis shows the momentum component of the measured electron in the direction of polarization (k_{ez1}) and the horizontal axis the same momentum component of the second electron. The data are integrated over the transverse momentum of the first and second electron. The momentum of the second electron is deduced from the measured momenta of the first electron and the recoiling ion by momentum conservation.

At 3.8×10^{14} W cm^{-2}, right at the 'knee' of the double ionization rate (see refs 19 and 25), a strong momentum correlation between the two electrons is found. There is a clear maximum for both electrons being emitted with the same momentum component of about 1 a.u., whereas emission to opposite half planes is strongly suppressed. At an intensity of 15×10^{14} W cm^{-2} (Fig. 2b), in the regime where the ratio of double to single ionization steeply rises with laser peak power, the correlation between the electrons is completely lost. Because only one component of the electron momenta is shown, Fig. 2a does not imply that the electrons are really emitted in parallel. More likely, there is an angle between the electrons owing to the repulsion.

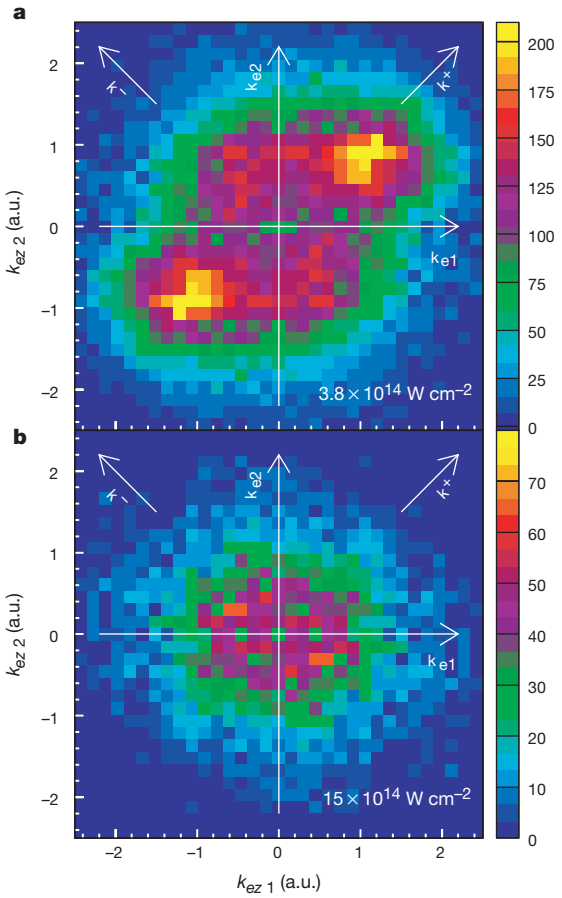

Figure 2 Momentum correlation between the two emitted electrons when an Ar^{2+} ion is produced in the focus of a 220-fs, 800-nm laser pulse at peak intensities of 3.8×10^{14} W cm^{-2} (**a**) and 15×10^{14} W cm^{-2} (**b**). The horizontal axis shows the momentum component of one electron along the polarization of the laser field; the vertical axis shows the same momentum component of the corresponding second electron. The same sign of the momenta for both electrons means emission to the same half sphere. The data are integrated over the momentum components in the direction perpendicular to the polarization. The colour coding shows the differential rate in arbitrary units.

The difference between Fig. 2a and b, which is accompanied by a sixfold increase in the ratio of double to single ionization[19,25], is a direct experimental proof for the change of mechanisms for double ionization as a function of laser power. In the region of the knee in the double ionization rate, the two-electron process is mediated by electron–electron correlation, whereas at high laser powers, double ionization proceeds by sequential emission of the two electrons. As there may be a random number of optical halfcycles between the emission of the two electrons in this case, no directional correlation between the electrons can be expected.

An instructive alternative perspective on Fig. 2 is obtained by rotating the distribution by 45°. The diagonal coordinate frame as indicated in the figure shows the sum and difference momenta $k^+ = k_1 + k_2$ and $k^- = k_1 - k_2$ of the individual electron momenta $k_{1,2}$. Owing to momentum conservation, k^+ is equal and opposite to the Ar^{2+} recoil-ion momentum (compare refs 18–20). Figure 2a shows that the width of the k^- distribution is narrower than the width in the k^+ direction. The coordinates k^+ and k^- are helpful to illustrate the relative importance of the two counteracting effects of electron–electron repulsion and acceleration of particles by the optical field. Both influence the observed final state momenta in different ways. Electron repulsion (and two-body electron–electron scattering) does not change k^+ but contributes to the momentum k^-. On the other hand, once both electrons are set free, the momentum transfer received from the field is identical. Therefore, this part of the acceleration does not change k^- but adds to k^+. The observed wide k^+ and narrow k^- distributions thus indicate that the joint acceleration of the electrons in the laser field clearly dominates over the influence of electron repulsion. Both electrons are driven by the laser field to the same side. This experimental finding is in agreement with theoretical results calculated using the model of the energy-sharing mechanism[26].

How does this finding relate to the two correlation mechanisms of re-scattering and shake-off? The pure case for the latter is found in single-photon double ionization, where the final state momentum distribution is predominantly determined by the long-range Coulomb interaction in the final state. It forces the electrons almost completely to opposite half spheres (see ref. 1 for a review). At small energies, which dominate in our case, k^+ is much smaller than k^- (see ref. 27). If a shake-off process were to take place in a strong laser field, it would set both electrons free in a time interval that would be very short compared with the optical cycle. Furthermore, shake-off would have its highest probability at the maximum intensity of the electric field, which is where single ionization also maximizes. After being set free the electrons perform a quiver motion in the field. The remaining net momentum transfer at the end of the laser pulse depends on the phase at which the electrons are set free. Ionization at the maximum of the field corresponds to zero net momentum transfer from the field. Therefore, the field is not expected to have a significant role in the final state electron momenta resulting from a shake-off. Such electrons should be found either close to the origin in Fig. 2 or in the region of opposite momenta due to electron repulsion. Thus Fig. 2a is in clear contradiction to the expectations of a shake-off model.

In the re-scattering or 'energy-sharing model', there is one particular process that produces electrons with similar momentum. If the energy of the primary electron at its re-encounter with the ion is equal to the energy needed to excite the second electron in the ion, the excitation process would stop the primary electron. The excited electron would then be set free with very little excess energy by the laser. Both electrons will finally have similar momentum which is only determined by the phase of the field at the re-encounter. The momentum of about 1 a.u. corresponds to a phase at re-scattering of 35° and a return energy of the primary electron of about 18 eV. This is sufficient for an excitation, as a broad band of many excited states of the Ar^+ ion starts at about 16.5 eV (the ionization energy is 27 eV). We conclude that the re-scattering model provides a

plausible scheme to produce the observed momentum correlation of the electrons.

Our measured momentum correlation shows that it is not the electron correlation in the initial ground state of the atom that leads to the enhanced double ionization in strong fields, but rather a re-scattering which is a result of the driving field. The magnitude of the momenta of the electrons in the direction of the laser field provides information on the phase of the field at the instant of recollision. The width of the distribution in the k^- direction is sensitive to the details of the re-scattering. Thus we expect that the momentum in the k^- direction and the momentum correlation in the directions perpendicular to the polarization will give further insight into the details of the correlation mechanism in future studies.

Finally, we note that the observed emission of the electrons to the same side confirms a prediction of Taylor *et al.*[28]. They have solved the time-dependent Schrödinger equation for two electrons in an optical field in three dimensions and found that most of the double ionization probability flux emerges to the same side. Similar conclusions have been drawn from one-dimensional model calculations[29,30].

The findings of this work provide a benchmark for theoretical efforts to calculate one of the most simple correlated two-electron processes in nature. Our method, using many-particle momentum space imaging for strong field physics, opens up the road for a variety of applications. The study of electron correlation in strong fields is now possible in molecules, clusters and solids (such as superconductors). □

Received 13 January; accepted 17 March 2000.

1. Briggs, J. S. & Schmidt, V. Differential cross sections for photo-double-ionization of the helium atom. *J. Phys. B* **33,** R1–R48 (2000).
2. Moshammer, R. *et al.* Double ionization of helium and neon for fast heavy-ion impact: Correlated motion of electrons from bound to continuum states. *Phys. Rev. Lett.* **77,** 1242–1245 (1996).
3. Lambropoulos, P., Maragakis, P. & Zhang, J. Two-electron atoms in strong fields. *Phys. Rep.* **305,** 203–293 (1998).
4. Fittinghoff, D. N., Bolton, P. R., Chang, B. & Kulander, K. C. Observation of nonsequential double ionization of helium with optical tunneling. *Phys. Rev. Lett.* **69,** 2642–2645 (1992).
5. Walker, B. *et al.* Precision measurement of strong field double ionization of helium. *Phys. Rev. Lett.* **73,** 1227–1231 (1994).
6. Corkum, P. B. Plasma perspective on strong field multiphoton ionization. *Phys. Rev. Lett.* **71,** 1994–1997 (1993).
7. Kulander, K. C., Cooper, J. & Schafer, K. J. Laser-assisted inelastic rescattering during above threshold ionization. *Phys. Rev. A* **51,** 561–568 (1995).
8. Liu, W. C., Eberly, J. H., Haan, S. L. & Grobe, R. Correlation effects in two-electron model atoms in intense laser fields. *Phys. Rev. Lett.* **85,** 520–523 (1999).
9. Watson, J. B., Sanpera, A., Lappas, D. G., Knight, P. L. & Burnett, K. Nonsequential double ionization of helium. *Phys. Rev. Lett.* **78,** 1884–1887 (1997).
10. Lappas, D. G. & van Leeuwen, R. Electron correlation effects in the double ionization of He. *J. Phys. B* **31,** L249–256 (1998).
11. LaGattuta, K. J. & Cohen, J. S. Quasiclassical modelling of helium double photoionisation. *J. Phys. B* **31,** 5281–5291 (1998).
12. Becker, A. & Faisal, F. H. M. Mechanism of laser-induced double ionization of helium. *J. Phys. B* **29,** L197–202 (1996).
13. Becker, A. & Faisal, F. H. M. S-matrix analysis of ionization yields of noble gas atoms at the focus of Ti:sapphire laser pulses. *J. Phys. B* **32,** L335–L343 (1999).
14. Schafer, K. J., Yang, B., DiMauro, L. F. & Kulander, K. C. Above threshold ionization beyond the high harmonic cutoff. *Phys. Rev. Lett.* **70,** 1599–1602 (1993).
15. Fittinghoff, D. N., Bolton, P. R., Chang, B. & Kulander, K. C. Polarization dependence of tunneling ionization of helium and neon by 120-fs pulses at 614 nm. *Phys. Rev. A* **49,** 2174–2177 (1994).
16. Sheehy, B., Lafon, R., Widmer, M., Walker, B. & DiMauro, L. F. Single- and multiple-electron dynamics in the strong-field tunneling limit. *Phys. Rev. A* **58,** 3942–3952 (1998).
17. Becker, A. & Faisal, F. H. M. Interplay of electron correlation and intense field dynamics in the double ionization of helium. *Phys. Rev. A* **59,** R1742–R1745 (1999).
18. Weber, T. *et al.* Recoil-ion momentum distributions for single and double ionization of helium in strong laser fields. *Phys. Rev. Lett.* **84,** 443–446 (2000).
19. Weber, T. *et al.* Sequential and nonsequential contributions to double ionization in strong laser fields. *J. Phys. B* **33,** L128–L133 (2000).
20. Moshammer, R. *et al.* Momentum distributions of Ne ions created by an intense ultrashort laser pulse. *Phys. Rev. Lett.* **84,** 447–450 (2000).
21. Dörner, R. *et al.* Cold target recoil ion momentum spectroscopy. *Phys. Rep.* **330,** 95–192 (2000).
22. Ullrich, J. *et al.* Cold target recoil ion momentum spectroscopy. *J. Phys. B* **30**, 2917–2974 (1997).
23. Dörner, R. *et al.* Photo double ionization of He: Fully differential and absolute electronic and ionic momentum distributions. *Phys. Rev. A* **57,** 1074–1090 (1998).
24. DiMauro, L. F. & Agostini, P. in *Advances in Atomic and Molecular Physics* 79–120 (Academic, New York, 1995).
25. Larochelle, S., Talebpour, A. & Chin, S. L. Non-sequential multiple ionization of rare gas atoms in a Ti:Sapphire laser field. *J. Phys. B* **31,** 1201–1214 (1998).
26. Becker, A. & Faisal, F. H. M. Interpretation of momentum distribution of recoil ions from laser induced non-sequential double ionization. *Phys. Rev. Lett.* **84,** 3546–3549 (2000).
27. Dörner, R. *et al.* Fully differential cross sections for double photoionization of He near threshold measured by recoil ion momentum spectroscopy. *Phys. Rev. Lett.* **77,** 1024–1027 (1996).
28. Taylor, K. T., Parker, J. S., Dundas, D., Smyth, E. & Vitirito, S. Laser driven helium in full-dimensionality. *Laser Phys.* **9,** 98–116 (1999).
29. Lein, M., Gross, E. K. U. & Engel, V. On the mechanism of strong-field double photoionisation in the helium atom. *J. Phys. B* **33,** 433–442 (2000).
30. Dörr, M. Double ionization in a one-cycle laser pulse. *Optics Express* **6,** 111–116 (2000).

Acknowledgements

We thank H. Schmidt-Böcking for enthusiastic support, and R. Moshammer and J. Ullrich for helpful discussons. Our analysis of the influence of the laser field on the final state momenta emerged after fruitful discussion with A. Becker and F. H. M. Faisal. We are grateful to W. W. Rühle for continuous support and thank Roentdek GmbH for providing the position sensitive detectors. This work is supported by DFG, BMBF, GSI and DAAD. R.D. is supported by the Heisenberg Programme of the DFG. The Marburg group thanks the Land Hessen and the DFG for support through the SFB383 and their Graduierten-kolleg 'Optoelektronik mesoskopischer Halbleiter'.

Correspondence and requests for materials should be addressed to R.D. (e-mail: doerner@hsb.uni-frankfurt.de).

Improving the performance of doped π-conjugated polymers for use in organic light-emitting diodes

Markus Gross*, David C. Müller*, Heinz-Georg Nothofer†, Ulrich Scherf†, Dieter Neher‡, Christoph Bräuchle* & Klaus Meerholz*

** Institut für Physikalische Chemie, Ludwig-Maximilian-Universität München, Butenandtstrasse 11, 81377 München, Germany*
† Max-Planck Institute für Polymerforschung, Institut Ackermannweg 10, 55037 Mainz, Germany
‡ Institut für Experimentalphysik, Universität Potsdam, Am Neuen Palais 10, 14469 Potsdam, Germany

Organic light-emitting diodes (OLEDs) represent a promising technology for large, flexible, lightweight, flat-panel displays[1–3]. Such devices consist of one or several semiconducting organic layer(s) sandwiched between two electrodes. When an electric field is applied, electrons are injected by the cathode into the lowest unoccupied molecular orbital of the adjacent molecules (simultaneously, holes are injected by the anode into the highest occupied molecular orbital). The two types of carriers migrate towards each other and a fraction of them recombine to form excitons, some of which decay radiatively to the ground state by spontaneous emission. Doped π-conjugated polymer layers improve the injection of holes in OLED devices[4–9]; this is thought to result from the more favourable work function of these injection layers compared with the more commonly used layer material (indium tin oxide). Here we demonstrate that by increasing the doping level of such polymers, the barrier to hole injection can be continuously reduced. The use of combinatorial devices allows us to quickly screen for the optimum doping level. We apply this concept in OLED devices with hole-limited electroluminescence (such as polyfluorene-based systems[10–12]), finding that it is possible to significantly reduce the operating voltage while improving the light output and efficiency.

OLED devices are typically fabricated using one transparent electrode. The material most commonly employed for this purpose is indium tin oxide (ITO), which serves as the anode. The electronic work function ϕ_w of ITO is generally smaller than the highest